# Free Energy Functionals for Efficient Phase Field Crystal Modeling of Structural Phase Transformations

Michael Greenwood,[1,2] Nikolas Provatas,[2] and Jörg Rottler[1]

[1]*Department of Physics and Astronomy, University of British Columbia, 6224 Agricultural Road Vancouver, British Columbia, V6T 1Z1, Canada*

[2]*Department of Materials Science and Engineering, McMaster University, 1280 Main Street West, Hamilton, Ontario, L8S 4L7, Canada*

(Received 30 December 2009; revised manuscript received 20 June 2010; published 23 July 2010)

The phase field crystal (PFC) method is a promising technique for modeling materials with atomic resolution on mesoscopic time scales. While numerically more efficient than classical density functional theory (CDFT), its single mode free energy limits the complexity of structural transformations that can be simulated. We introduce a new PFC model inspired by CDFT, which uses a systematic construction of two-particle correlation functions that allows for a broad class of structural transformations. Our approach considers planar spacings, lattice symmetries, planar atomic densities, and atomic vibrational amplitudes in the unit cell, and parameterizes temperature and anisotropic surface energies. The power of our approach is demonstrated by two examples of structural phase transformations.

DOI: 10.1103/PhysRevLett.105.045702 PACS numbers: 64.70.K−, 46.15.−x, 61.50.Ah, 81.10.Aj

Solid-state transformations involve structural changes that couple atomic-scale elastic and plastic effects with diffusional processes [1–3]. These phenomena are presently impossible to compute at experimentally relevant time scales using molecular dynamics simulations. On the other hand, mesoscale continuum models wash out most of the relevant atomic-scale physics that leads to elasticity, plasticity, defect interactions, and grain boundary nucleation and migration. Traditional phase field studies of precipitate and ledge growth [3,4] thus introduce these effects phenomenologically. To our knowledge, there are no phase field models presently available that self-consistently model polycrystalline interactions and elastic and plastic effects at the atomic scale.

Classical density function theory (CDFT) provides a formalism that describes the emergence of crystalline order from a liquid or solid phase through a coarse-grained density field [5]. Unfortunately, it requires high spatial resolution and is inefficient for dynamical calculations [6] due to sharp density spikes in the solid phases. The recently introduced phase field crystal (PFC) model has been gaining widespread recognition as a hybrid method between CDFT and traditional phase field methods. This new formalism captures the essential physics of CDFT without having to resolve the sharp atomic density peaks [7–11]. Despite their success, existing PFC free energies allow for only a limited range of structural transformations between different crystalline states. Moreover, extensions of the original PFC concept to crystal symmetries such as square [12,13] and fcc [6,14,15] have been somewhat *ad hoc* and not self-consistently connected to material properties.

This Letter proposes an extension of the PFC model by systematically constructing phenomenological kernels with energy minima for targeted crystalline states. Our approach preserves the PFC model's numerical efficiency, and its utility is demonstrated by dynamically simulating the growth of solid phases into a liquid and the nucleation of precipitate phases within a parent phase of different crystallographic symmetry. We begin with a free energy functional,

$$\Delta F[n(\vec{r})] = \Delta F_{\mathrm{id}}[n(\vec{r})] + \Delta F_{\mathrm{ex}}[n(\vec{r})], \tag{1}$$

where $\Delta F$ is the free energy difference with respect to a uniform reference density $\rho_0$ [16], and has contributions from a noninteracting term $\Delta F_{\mathrm{id}}$ and an excess energy $\Delta F_{\mathrm{ex}}$ responsible for the formation of structured phases.

Equation (1) is expanded around the uniform reference density using the dimensionless number density $n(\vec{r}) = \rho(\vec{r})/\rho_o - 1$, where $\rho(\vec{r})$ is the coarse-grained local density. The ideal contribution to the energy is approximated by expanding the Helmholtz free energy of an ideal gas,

$$\begin{aligned}\Delta F_{\mathrm{id}} &= \rho_o k_B T \int d\vec{r}[1 + n(\vec{r})]\ln[1 + n(\vec{r})] - n(\vec{r}) \\ &\approx \rho_o k_B T \int d\vec{r}\left[\frac{n(\vec{r})^2}{2} - \frac{n(\vec{r})^3}{6} + \frac{n(\vec{r})^4}{12}\right].\end{aligned} \tag{2}$$

The excess energy is expanded to include only second order correlations [9,16–18],

$$\Delta F_{\mathrm{ex}} = -\frac{\rho_o k_B T}{2} \int d\vec{r} n(\vec{r}) \int d\vec{r}'[C_2(|r - r'|)n(\vec{r}')], \tag{3}$$

where $C_2(|\vec{r} - \vec{r}'|)$ plays the role of a two-particle direct correlation function. The PFC model evolves the dimensionless number density field $n(\vec{r})$ in time using the typical conserved dissipative dynamics [7], $\frac{\partial n(\vec{r})}{\partial t} = M\nabla^2[\delta\Delta F/\delta n(\vec{r})] + A_n\nabla^2\eta$ where $M$ is a kinetic mobility parameter and conserved noise $\eta$ with an amplitude of $A_n$ is added to facilitate nucleation from metastable

 

states [7,19]. Equation (3) is integrated in reciprocal space using a semi-implicit technique [8,11].

Periodic structures emerge in the PFC model by the introduction of the kernel $C_2(k)$ that results in free energy minima corresponding to particular modes in the density field. Here we do not aim to construct such kernels from first principles, but rather seek the simplest possible forms that result in the desired crystal structure. To this end, we expand the free energy functional about a uniform reference density [18] and choose modes in the correlation functions that will create an energy minimum for the desired structure. The original PFC model by contrast uses only a single mode [7]. Figure 1 shows two examples of direct pair correlation functions that produce stable square (a) and simple cubic (sc) (b) lattices for minimized free energies. The functions $C_2(k)$ are constructed in reciprocal space by combining multiple peaks whose position, amplitude, and width are determined as follows:

The number and position of peaks in the reciprocal space correlation function is determined by the desired unit cell. In diffraction theory a reciprocal lattice has families of peaks derived from the interplanar spacings. For a 2D square lattice, for instance, the unit cell contains two families of planes, {10} and {11}, with spacings $\lambda_1$ and $\lambda_2$ as shown in the inset of Fig. 1(a). For a perfect crystal, there are an infinite number of peaks located at integer

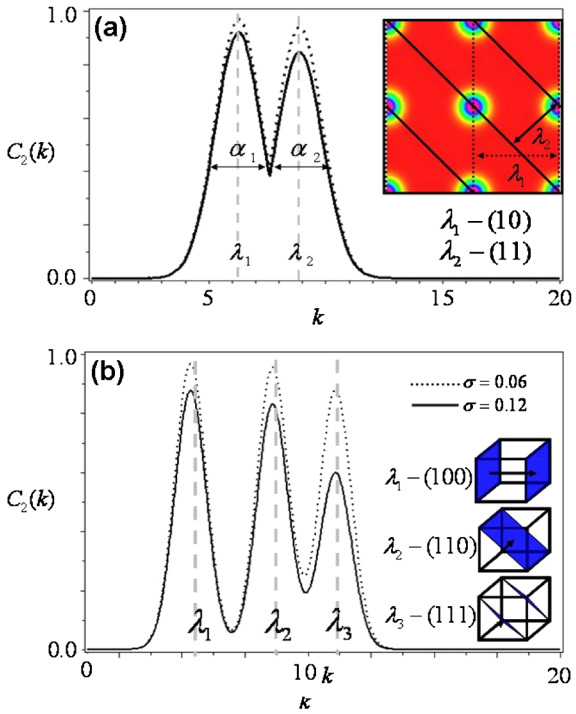


FIG. 1 (color online). (a) Direct pair correlation function for a square lattice at two effective temperatures ($\sigma = 0.82$, solid and $\sigma = 0.5$, dotted, see text). The two peaks in the correlation function each represent one of two planes in the unit cell with interplanar spacings $\lambda_1$ and $\lambda_2$ (see inset). (b) Correlation function for a simple cubic (sc) lattice at two different temperatures. In 3D, a cubic lattice is represented by three planes in the unit cell.

multiples of the wave vector $k_i = 2\pi/\lambda_i$, where $i$ denotes the plane. For square and cubic lattices, it is sufficient, in our PFC formalism, to keep only the lowest frequency mode for each family of these peaks in the correlation function.

Temperature enters our correlation function via modulation of the peak heights by a factor $e^{-\sigma^2 k_i^2/2\rho_i\beta_i}$, where the effective temperature $\sigma$ acts as a control parameter. The form of this term is motivated by the effect of thermal motion of atoms about their equilibrium positions with amplitude $\sigma_v$, which modulates the scattering intensity by a Debye-Waller-Factor $e^{-\sigma_v^2 k_i^2/2}$. The peak heights in the correlation function are additionally influenced by the (dimensionless) atomic density $\rho_i$ within a plane and the number of planes $\beta_i$ in each family. We therefore enter these effects into the excess energy phenomenologically by modulating the peaks in $C_2(k)$ with a factor $\exp[-\frac{\sigma^2 k_i^2}{2\rho_i\beta_i}]$. For example, in a square lattice the families of {11} and {10} planes each consist of 4 sets of planes [i.e., the {11} family contains (11), $(\bar{1}1)$, $(1\bar{1})$, and $(\bar{1}\,\bar{1})$] and therefore $\beta_{11} = \beta_{10} = 4$. The (11) plane has an atomic density $\rho_{11} = 1/\sqrt{2}$ and the (10) plane has a density of $\rho_{10} = 1$. Incorporating both the decay of correlation peak heights through an effective temperature $\sigma$ and the inclusion of only the lowest frequency peaks of each family of planes in the excess energy leads to the broad real-space density peaks that give this model its numerical efficiency.

The peaks in the reciprocal space correlation function are represented by Gaussians $\exp[-\frac{(k-k_i)^2}{2\alpha_i^2}]$ of finite width $\alpha_i$ rather than the $\delta$—peaks of a perfect lattice. The parameter $\alpha_i$ accounts for changes in the free energy due to interfaces, defects, and strain. Varying $\alpha_i$ changes the width of a liquid-solid interface, which directly affects the surface energy [20]. The relationship between the interface width and the peak width in the correlation function is $1/\alpha_i \propto W_i$ as illustrated in Fig. 2. This result can be arrived at by the inverse Fourier transform of $C_2(k)$ and agrees well with the traditional phase field models, which incorporate surface energy through square gradient terms in the order parameter.

In summary, each family of planes $i$ in the unit cell contributes a peak to the kernel in the form of $C_2(k)_i = \exp[-(\sigma^2 k_i^2)/(2\rho_i\beta_i)]\exp\{-[(k-k_i)^2]/(2\alpha_i^2)\}$. To further simplify the construction, the correlation functions in this work (Fig. 1) comprise the numerical envelope of the superposition of all relevant peaks for the crystal structure, to avoid shifts in the peak positions and correspondingly changes to the stable structure that would result from a simple sum. This provides a general and robust method by which to generate desired crystal structures, incorporating temperature dependence through modulation of the correlation peak heights. Through the use of $\alpha_1$ and $\alpha_2$ we can also change the anisotropy of a given crystal structure.

The phase diagram is constructed from the free energy curves obtained for each bulk phase. Free energy curves

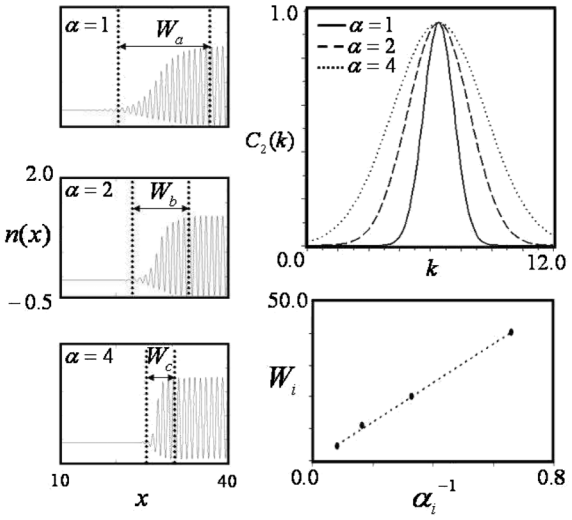


FIG. 2. Effect of peak width $\alpha_i$ in the correlation functions on planar interface width $W_i$. Left: Three values of $\alpha_i$ and their resulting interface widths. Top right: Peak shapes corresponding the interface widths to the left. Bottom right: Dependence of simulated interface width on the correlation peak width (see text).

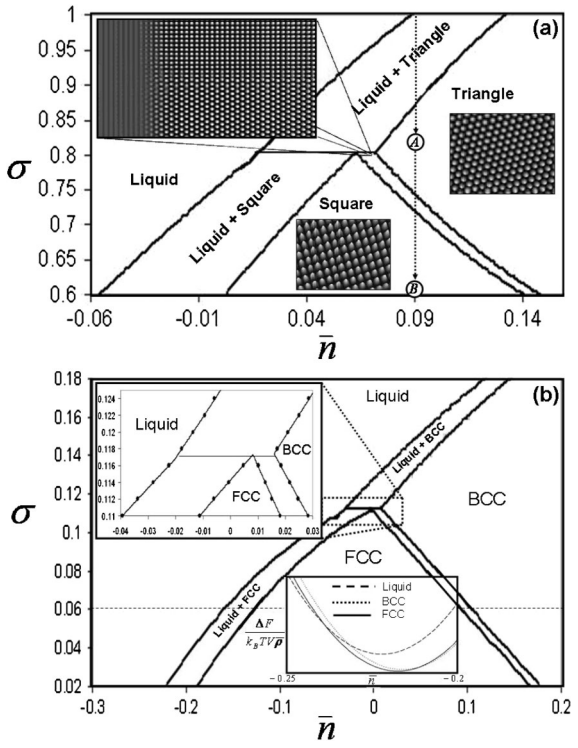


FIG. 3. (a) Phase diagram for a square lattice correlation function showing coexistence between liquid, solid, and triangular phases. The inset contains stripes of square and triangular lattices in a liquid phase quenched to a temperature $\sigma = 0.79$. The square phase density was initialized to $n_{\mathrm{sq}} = 0.067$ and the triangular phase density to $n_{\mathrm{tri}} = 0.076$. The mean density of the system is set to $\bar{n} = 0.07$ and the surface energy parameters are $\alpha_1 = \sqrt{2}$ and $\alpha_2 = 1$. (b) Phase diagram for a fcc correlation function. The insets show the peritectic point and the energy curves for the liquid, fcc and bcc states at $\sigma = 0.06$.

are calculated by an iterative relaxation technique for each structure using the kernel for the structure of interest. For the liquid state, the energy is calculated by imposing a constant density field, and the energy per unit volume is calculated by numerically integrating Eq. (1). For the solid state, the structures corresponding to the correlation function are fit using a Gaussian density field and then relaxed. For example, for the correlation function of Fig. 1(a), density fields for square and triangular lattices with lattice spacings of 1 and $2/\sqrt{3}$ are relaxed using the conserved dynamics to allow density peaks to obtain an amplitude corresponding to the local minimum energy state. This process is repeated for a series of mean densities to produce energy-density curves for each phase at a given effective temperature $\sigma$ [Fig. 3(b), inset]. The double tangent construction is performed for many values of $\sigma$, giving the phase diagrams in Fig. 3(a) for the square correlation function and in Fig. 3(b) for the fcc correlation function.

In both 2D and 3D, the phase that possesses the symmetry of the underlying correlation function emerges at low temperatures and intermediate densities. As the effective temperature is increased the lower frequency modes of the correlation function dominate over the higher frequency modes, which changes the particular structure that minimizes the free energy. For example, the square (fcc) crystal transforms into a triangular (bcc) crystal since the triangular (bcc) structure minimizes the energy in the single mode approximation. Note that our model also predicts transformation of coexisting liquid and solid phases into a new single solid phase at a peritectic point in both two and three dimensions. This remarkable feature opens an important window into the study of structural phase transformations. Coexistence between fcc crystals with the liquid phase is also obtained, as is coexistence of the liquid and sc phases using the kernel shown in Fig. 1(b).

Our model is applied to two important examples of solid-state processes using the phase diagram of Fig. 3. The first is the growth of two structurally different lattices in coexistence, initialized in rectangular domains, into a liquid phase as illustrated in the inset of Fig. 3(a). The square phase is oriented such that the {10} planes are in contact with the liquid phase. Since each peak in the two-particle correlation function represents a single family of planes, the surface energy of the interface of the square phase {10}-facet is derived from the width $\alpha_2$ of the second peak of the correlation function, while the surface energy of triangular phase facets are derived directly from the width $\alpha_1$ of the first peak. Anisotropy of surface energy can be controlled by increasing or decreasing $\alpha_1$ while holding $\alpha_2$ constant. This effect also extends to the solid-solid surfaces between boundaries of different structure (for example, triangle-square boundaries). The triangle structure is derived directly from a single mode approximation, therefore the magnitude of the anisotropy is deter-

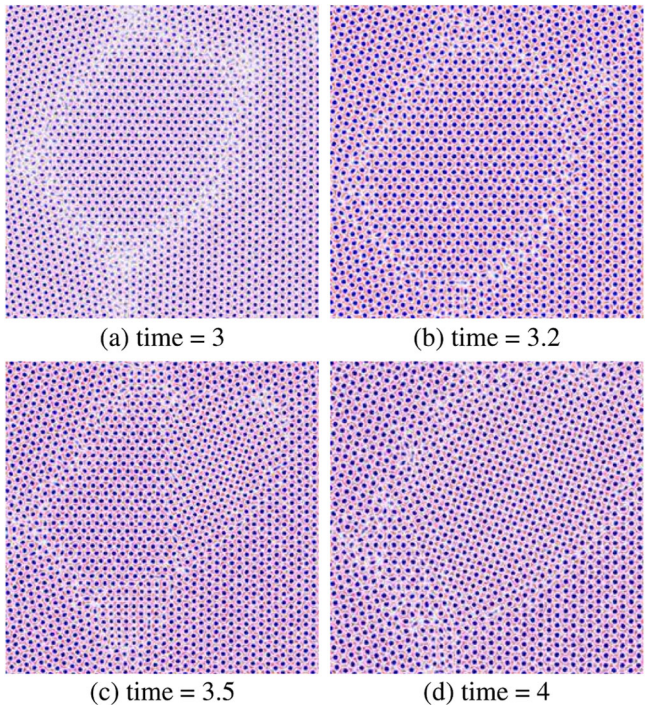


FIG. 4 (color online). 2D nucleation from triangles to squares with noise amplitude of $A_n = 0.01$ (a) A liquid with density $\bar{n} = 0.09$ is quenched into the triangular region of the phase diagram ($\sigma = 0.82$), marked ($A$) in Fig. 3(a), produces grains with triangular symmetry. (b)–(d) A further quench into the square portion of the phase diagram ($\sigma = 0.6$), marked ($B$) in Fig. 3(a), illustrating the nucleation and subsequent growth of square grains at the vertices of the triangular grains.

mined strictly by the underlying structure. Small changes in the strength of the anisotropy lead to small changes in the angle of the solid liquid interfaces at vertices between the three phases.

The second application of interest is the nucleation of a structural phase by a quench into the second phase region of the phase diagram. To illustrative this, the simple 2D case of square-triangle structural transformations is shown here. A liquid with a homogeneous density field is quenched into the triangular region of the phase diagram [point $A$ on the quench path in Fig. 3(a)]. Small amplitude noise facilitates the nucleation of randomly oriented triangular phase seeds in the liquid phase. These seeds grow, impinge and coarsen over time. A small grain is illustrated in Fig. 4(a). After the triangular grains undergo some coarsening, the material is quenched into the square portion of the phase diagram (point $B$). A thermodynamic driving force leads to the nucleation, growth, and coarsening of the square phase. The nucleation events occur at vertex positions in the triangular grain structures, as observed in experiments [1]. The driving force for the transformation is greatest at these positions and can overcome the nucleation barrier. Two such nucleation points are shown in Fig. 4(b). The orientation of a nucleus and coherency strains can inhibit the growth of the new phase that precipitates, eventually to be dominated by another more favorable precipitate. This effect is illustrated in panels (c) and (d) of Fig. 4. These results demonstrate that our approach is capable of modeling the distribution of square or fcc precipitate orientations, an important phenomenon that can be compared to experiments.

We introduced new PFC free energy functionals for efficient numerical study of solid-state transformations. In contrast to earlier work [13], we find that two-point correlations are sufficient to generate stable cubic lattices, and higher order terms in the expansion of $\Delta F_{ex}$ can still be neglected. The correlation functions are systematically built up from fundamental principles and desired crystallographic properties of phases of interest at a finite temperature. Our approach can model peritectic transitions as well as the nucleation and growth of second-phase precipitates with different crystalline structures. Our model can be validated against numerous experiments, as well as MD simulations of triple junctions.

This work has been supported by the Natural Science and Engineering Research Council of Canada (NSERC).

[1] J. W. Martin, R. D. Doherty, and B. Cantor, *Stability of Microstructure in Metallic Systems* (Cambridge University Press, Cambridge, 1997), 2nd ed.
[2] F. Liu, F. Sommer, and E. Mittemeijer, Int. Mater. Rev. **52**, 193 (2007).
[3] J. Zhu, T. Wang, A. Ardell, S. Zhou, Z. Liu, and L. Chen, Acta Mater. **52**, 2837 (2004).
[4] M. Greenwood, J. Hoyt, and N. Provatas, Acta Mater. **57**, 2613 (2009).
[5] H. Lowen, Phys. Rep. **237**, 249 (1994).
[6] A. Jaatinen, C. V. Achim, K. R. Elder, and T. Ala-Nissila, Phys. Rev. E **80**, 031602 (2009).
[7] K. R. Elder, M. Katakowski, M. Haataja, and M. Grant, Phys. Rev. Lett. **88**, 245701 (2002).
[8] K. R. Elder and M. Grant, Phys. Rev. E **70**, 051605 (2004).
[9] K. R. Elder, N. Provatas, J. Berry, P. Stefanovic, and M. Grant, Phys. Rev. B **75**, 064107 (2007).
[10] P. Stefanovic, M. Haataja, and N. Provatas, Phys. Rev. Lett. **96**, 225504 (2006).
[11] J. Mellenthin, A. Karma, and M. Plapp, Phys. Rev. B **78**, 184110 (2008).
[12] J. Kröger, Masters thesis, McGill University, 2005.
[13] P. Tupper and M. Grant, Europhys. Lett. **81**, 40007 (2008).
[14] K.-A. Wu, Ph. D. thesis, Northeastern University, 2006.
[15] G. Tegze, L. Granasy, G. I. Toth, F. Podmaniczky, A. Jaatinen, T. Ala-Nissila, and T. Pusztai, Phys. Rev. Lett. **103**, 035702 (2009).
[16] T. V. Ramakrishnan and M. Yussouff, Phys. Rev. B **19**, 2775 (1979).
[17] S. van Teeffelen, R. Backofen, A. Voigt, and H. Löwen, Phys. Rev. E **79**, 051404 (2009).
[18] C. Ebner, H. R. Krishnamurthy, and R. Pandit, Phys. Rev. A **43**, 4355 (1991).
[19] A. Archer and M. Rauscher, J. Phys. A **37**, 9325 (2004).
[20] S. Majaniemi and N. Provatas, Phys. Rev. E **79**, 011607 (2009).